RSC Advances

PAPER

View Article Online
View Journal | View Issue

Cite this: *RSC Adv.*, 2016, **6**, 101974

Microfluidic chip-based one-step fabrication of an artificial photosystem I for photocatalytic cofactor regeneration†

Xiaowen Huang,[ac] Jian Liu,[b] Qingjing Yang,[d] Yang Liu,[ac] Yujiao Zhu,[ac] Tenghao Li,[ac] Yuen Hong Tsang[ac] and Xuming Zhang*[ac]

We propose herein, a one-step method to assemble the immobilized artificial photosystem I (IAPSI) in a microfluidic chip, which integrated a preformed graphitic carbon nitride photocatalyst (g-C_3N_4) and electron mediator (M) in one chip and mimicked the characteristics of photosystem I. The simultaneous assembly of g-C_3N_4 and M could efficiently regenerate NADH from NAD^+ under visible light irradiation, which verified the effectiveness of the assembly method. The *in situ* assembly method was thought to outperform traditional methods in several aspects in terms of facile synthesis, promotion of the combination of g-C_3N_4 and M through $\pi-\pi$ stacking and an enhanced coenzyme regeneration rate. For comparison, we used the bulk g-C_3N_4–slurry and the few-layer g-C_3N_4–slurry system as the control to regenerate the photocatalytic cofactor/coenzyme NADH, and measured the required times of 305 s and 30 s, respectively, to accomplish 63% NAD^+ conversion. In contrast, our IAPSI microreactor takes only 13 s, faster than the other two by factors of 23 and 2.3 times. Therefore, we assert that the simple, yet highly efficient nature of this technique can act as an important method for artificial photosynthesis, particularly in the photocatalytic cofactor recycling systems for the production of various valuable molecules.

Received 25th August 2016
Accepted 6th October 2016

DOI: 10.1039/c6ra21390a

www.rsc.org/advances

1 Introduction

Solar energy is the most abundant energy on earth.[1,2] One of the challenges for building a sustainable society is to develop practical materials and devices that can perform solar energy conversion (*i.e.*, solar fuel or solar electricity).[3–12] Natural photosynthesis is the fundamental process used by plants, algae and certain bacteria to harness energy from sunlight and convert it into chemical energy.[13] In the light reaction of natural photosynthesis, through a series of photo-induced electron transfer processes in photosystem I (PSI), an integral membrane protein complex in photosynthesis, the solar energy (photons) is firstly transferred into active electrons and is then used to reduce the coenzyme nicotinamide adenine dinucleotide phosphate ($NADP^+$) to NADPH.[14,15] In view of the importance of NAD(P)H/$NAD(P)^+$ in many biochemical conversions, particularly in many enzymatic redox reactions, mimicking such a process could provide a new way to design high-efficiency materials and devices for artificial photosynthesis.[16–18]

The efficiency of photosynthesis in plants is based on the high surface-area-to-volume ratio structures of PSI (Fig. 1A) including a series of light-harvesting complexes, several metal–protein clusters and a group of redox biocatalysts, which are logically integrated in the phospholipid bilayer and confined to certain areas. These immobilized structural features not only facilitate efficient electron transfer and enhanced photon absorption, but also the isolation of the reaction substrates and products providing an ordered reaction chain. Thus, by mimicking the function of the PSI system, the regeneration of coenzymes (NADH, NADPH) through solar energy is a promising, sustainable and economic strategy that has attracted many research efforts that have contributed to important improvements.[19–21] However, in the past, most of the work has focused on the heterogeneous photocatalysis for NADH regeneration, which renders the practical application impossible due to separation and recycling problems. Therefore, it is promising to develop a high-efficiency PSI artificial photosynthesis system on the immobilized system (IAPSI) for coenzyme regeneration, which would pave the way for practical uses in the near future.

Microfluidics, as versatile and promising systems, have several merits to benefit artificial photosynthesis in many ways.[22] They have the advantages of large surface areas, short

[a]Department of Applied Physics, The Hong Kong Polytechnic University, Hong Kong, P. R. China. E-mail: apzhang@polyu.edu.hk; Fax: +852-23337629; Tel: +852-4003258
[b]Department of Chemistry, Northwestern University, Evanston, Illinois 60208, USA
[c]The Hong Kong Polytechnic University Shenzhen Research Institute, Shenzhen, P. R. China
[d]Department of Applied Biology and Chemical Technology, Hong Kong Polytechnic University, Hong Kong, PR China

† Electronic supplementary information (ESI) available. See DOI: 10.1039/c6ra21390a

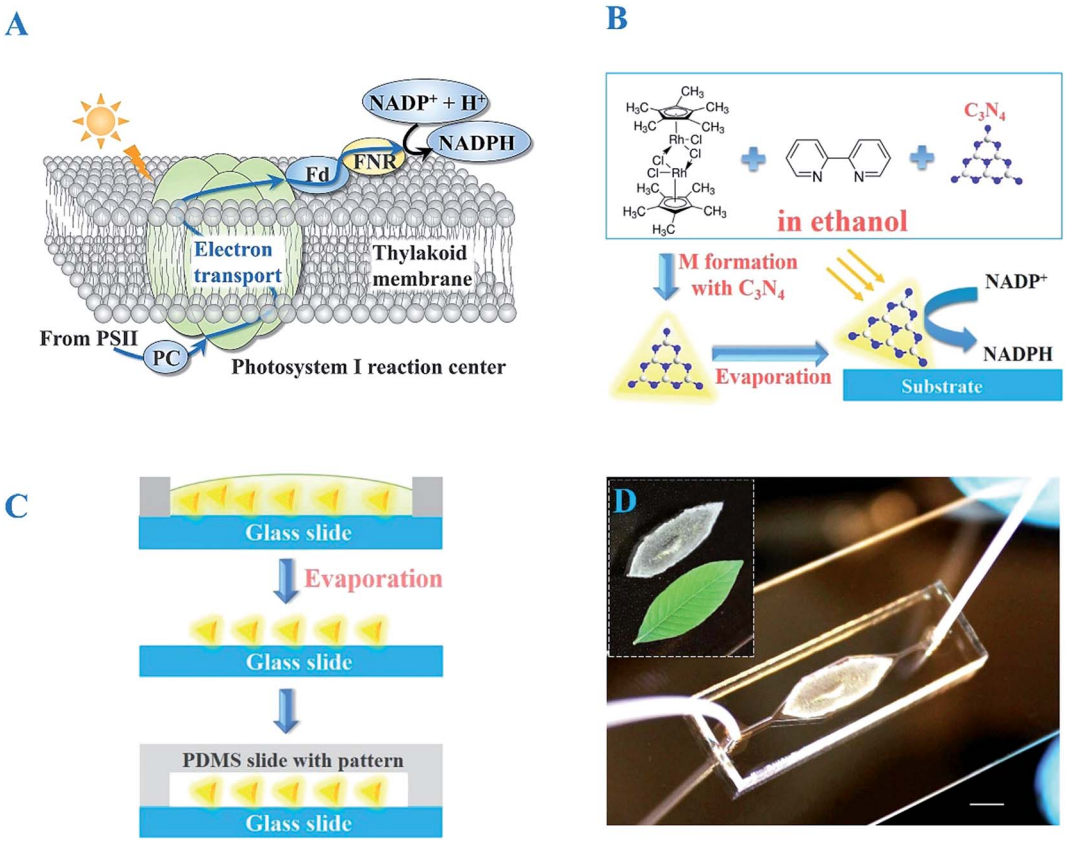

Fig. 1 (A) Schematic of the photosystem I reaction center. (B) One-step fabrication process of the immobilized artificial photosystem I (IAPSI) in the form of the g-C_3N_4–M film. (C) Simple procedures to fabricate the IAPSI microreactor. (D) Photograph of the as-fabricated IAPSI microreactor, in which the inset presents the leaf-like shape of g-C_3N_4–M. The scale bar is 2 mm in all figures.

diffusion lengths and uniform irradiation. In addition, they have been shown to enable quick tests of photocatalysts, optimization of the operating conditions and rapid screening of various photocatalysts due to the merits of their wide tunability and parallel analysis.[23,24] Moreover, compared with the conventional bulk slurry reactors that involve large reaction plates, microfluidics accommodates small volumes of fluids, resulting in low consumption of photocatalyst materials and samples.[25] This is particularly important for rare or expensive reaction chemicals.

Metal-free efficient photocatalysts have attracted much attention in artificial photosynthesis,[20,26,27] particularly the easily fabricated g-C_3N_4,[7,28,29] which is an earth-abundant and low-cost photocatalyst obtained from heating melamine or urea. Importantly, the π–π stacking interaction between the adenine subunit of β-NAD^+ and the electron-rich g-C_3N_4 promotes β-NAD^+ to attach to the layered g-C_3N_4.[15] Similarly, the π–π stacking interaction facilitates g-C_3N_4 to bind with the electron mediator, pentamethylcyclopentadienyl rhodium bipyridine {M, [Cp*Rh(bpy)Cl]Cl}, improving the transfer of electrons from the photocatalyst to the electron mediator. All of these advantages prompted us to choose g-C_3N_4 as the photocatalyst to fabricate the immobilized artificial PSI. Conventional methods to fabricate the IAPSI usually involve at least three steps: (1) the immobilization of the photocatalyst,[17,19,30] (2) the synthesis of an electron mediator M, and (3) the introduction of a suitable mediator to the reaction system. In fact, the presence of an excessive mediator usually harms the enzyme activity thereby decreasing the reaction efficiency.[31] Oppelt *et al.* proposed a smart and simple way to synthesize an IAPSI system immobilized on glass beads by coupling a light-harvesting ligand [2,2′-bipyridyl-containing poly(arylene-ethynylene)-*alt*-poly(arylene-vinylene)], with an organometallic rhodium complex for photocatalytic NAD^+/NADH reduction.[32] The NADH regeneration rate was only 21% at 26 h. Therefore, a system with a higher regeneration rate was required.

Herein, based on the merits of microfluidics, we proposed a simple one-step method in the microfluidic chip to simplify the processes and to improve the regeneration rate.[25,33] In this method, the typical three steps for the formation of the artificial PSI were integrated into one, thereby saving processing time. In addition, this method also possesses other advantages such as (1) facile synthesis, which reduces the dependence on many types of instruments, (2) promotion of the π–π stacking interaction because M is formed and stored with the existing g-C_3N_4, increasing the chance of a π–π stacking interaction, and (3) a higher coenzyme regeneration rate than that of the slurry method. All of these merits proved this method useful, efficient and with significant improvements.

2 Materials and methods

2.1 Synthesis of few-layer g-C_3N_4

For few-layer g-C_3N_4 synthesis, we firstly synthesized the bulk g-C_3N_4 powder according to a procedure described in a previous paper.[7] In detail, dicyandiamide (Aldrich, 99%) was heated at 550 °C for 4 h in static air with a ramp rate of 2.3 °C min^{-1}. The cooling rate was kept at around 1 °C min^{-1}. The resultant yellow agglomerates were milled into powder in a mortar. Then, through thermal oxidation etching of the bulk g-C_3N_4, few-layer g-C_3N_4 was prepared.[34] A 400 mg amount of the bulk g-C_3N_4 was placed in an open ceramic container followed by a heating process at 500 °C for 2 h with a ramp rate of 5 °C min^{-1}. Few-layer g-C_3N_4 was obtained as a light yellow powder.

2.2 Material characterization

The FTIR spectrum was collected using a Vertex 70 FTIR spectrometer (Bruker Corporation). XRD measurements were performed on a D8 Diffractometer from Bruker Instruments. The TEM images were obtained from a TEM grid to perform high-resolution morphology characterization using a JEM2100F TEM system operating at 200 kV. The atomic force microscope (AFM) image was obtained by the MFP-3D (Asylum Research). The photoluminescence (PL) spectra were measured by a F-4600 fluorescence spectrometer (Hitachi, Japan) with an excitation wavelength of 365 nm (room temperature). The UV-vis absorbance spectra were recorded using a UV2550 spectrophotometer (Shimadzu Scientific Instruments). The electron mediator structure was determined by nuclear magnetic resonance analysis (300 MHz, Bruker, Germany).

2.3 Microfluidic device fabrication

The PDMS layer with a simple leaf-like pattern (*i.e.*, the narrowest part is 400 μm and the widest part is 4200 μm with a height of 40 μm) was fabricated using the standard soft lithography technique.[35,36] In detail, we firstly designed a leaf-like photomask and obtained the corresponding SU-8 mold with selective exposure of UV-light. Then, we poured the uncrosslinked PDMS (10 : 1) on the mold. After a degassing and heating process (80 °C, 10 min), the PDMS layer with a leaf-like pattern was prepared.

2.4 IAPSI fabrication

The IAPSI fabrication process simply consisted of two steps, as shown in Fig. 1B. Step one involved mixing pentamethylcyclopentadienylrhodium(III) chloride dimer, 2,2′-bipyridyl and g-C_3N_4 together in ethanol. Thus, M [Cp*Rh(bpy)Cl]Cl was formed with g-C_3N_4. In step two, ethanol was removed by evaporation at 50 °C. The remaining part was IAPSI containing photocatalysts and electron mediator. Based on the merits of the microfluidic chip, we performed the photocatalytic cofactor regeneration in a microfluidic channel. Fig. 1C shows the simple IAPSI-microreactor fabrication process including the formation of IAPSI and covering the PDMS slide with a leaf-like pattern on it. This final fabricated microfluidic chip (40 μm high) is shown in Fig. 1D where the inset illustrates the leaf-like shape of g-C_3N_4–M.

The traditional way to synthesize M [Cp*Rh(bpy)Cl]Cl was to reflux a mixture of $RhCl_3 \cdot 3H_2O$ and one equivalent of 1,2,3,4,5-pentamethylcyclopentadiene in methanol for 24 hours. The resulting red precipitate was filtered and suspended in methanol. On addition of two equivalents of 2,2-bipyridine, the suspension cleared up and a yellowish solution was formed. The remaining oily red crystals were extracted with chloroform and the solution was dried over anhydrous magnesium sulphate. After evaporation under reduced pressure, the residue was recrystallized from chloroform–benzene. The product was dissolved in methanol and with the addition of two equivalents of 2,2′-bipyridine. Then, [Cp*Rh(bpy)Cl]Cl was precipitated by the addition of diethyl ether and the final compound was dissolved in water turning to $[Cp^*Rh(bpy)H_2O]^{2+}$. Obtaining electrons from photocatalysts, $[Cp^*Rh(bpy)H_2O]^{2+}$ allows the simultaneous transfer of $2e^-$ and $1H^+$ to NAD^+, resulting in the formation of NADH (*i.e.*, photocatalytic cofactor regeneration).

2.5 NADH photoregeneration

Photoregeneration of NADH was carried out by filling the microfluidic channel with 4 μL of reaction medium irradiated with a xenon lamp (300 W) through a 420 nm cut-off filter, avoiding the UV light-induced damage of the enzyme. The reaction medium (pH 8.0) was composed of NAD^+ (0.2 mM), TEOA (15 w/v%), and phosphate buffer (100 mM). A 4 μL aliquot of the reaction medium was filled into the prepared microfluidic chip. 20 μg of g-C_3N_4 was immobilized in each chip and the complex M was equal to 0.25 mM.

3 Results and discussion

3.1 Few-layer g-C_3N_4 characterization

We characterized the few-layer g-C_3N_4 by Fourier transform infrared spectroscopy (FTIR), X-ray diffraction (XRD), UV-vis absorption spectrometry, transmission electron microscopy (TEM) and scanning electron microscopy (SEM). Fig. 2A shows the FTIR spectrum of the few-layer g-C_3N_4. The broad peaks between 3000 and 3500 cm^{-1} are attributed to the N–H band. The peaks at 1251, 1325, 1419, 1571, and 1639 cm^{-1} correspond to the typical stretching modes of C–N heterocycles. The peak at 810 cm^{-1} corresponds to the characteristic breathing mode of triazine units, which is compliant with the reported data.[37] The few-layer g-C_3N_4 gives two XRD peaks at 12.7° and 27.8°, separately (Fig. 2B). The former one is the low-angle reflection peak, stemming from the lattice planes parallel to the *c*-axis and the later one is due to the stacking of the conjugated aromatic system. The UV-vis absorption spectrum of the few-layer g-C_3N_4 is broad, ranging from UV light to visible light (see Fig. 2C). The blue line in Fig. 2C is at the position of 420 nm, on the right of which can be seen the visible light absorption ability of g-C_3N_4. From the Tauc plot, the optical band gap of this g-C_3N_4 can be determined to be 2.9 eV from the $(\alpha h\nu)^2$ *versus* $h\nu$ graph, in which α, h and ν are the absorption coefficient, the Planck constant, and the light frequency, respectively. The optical

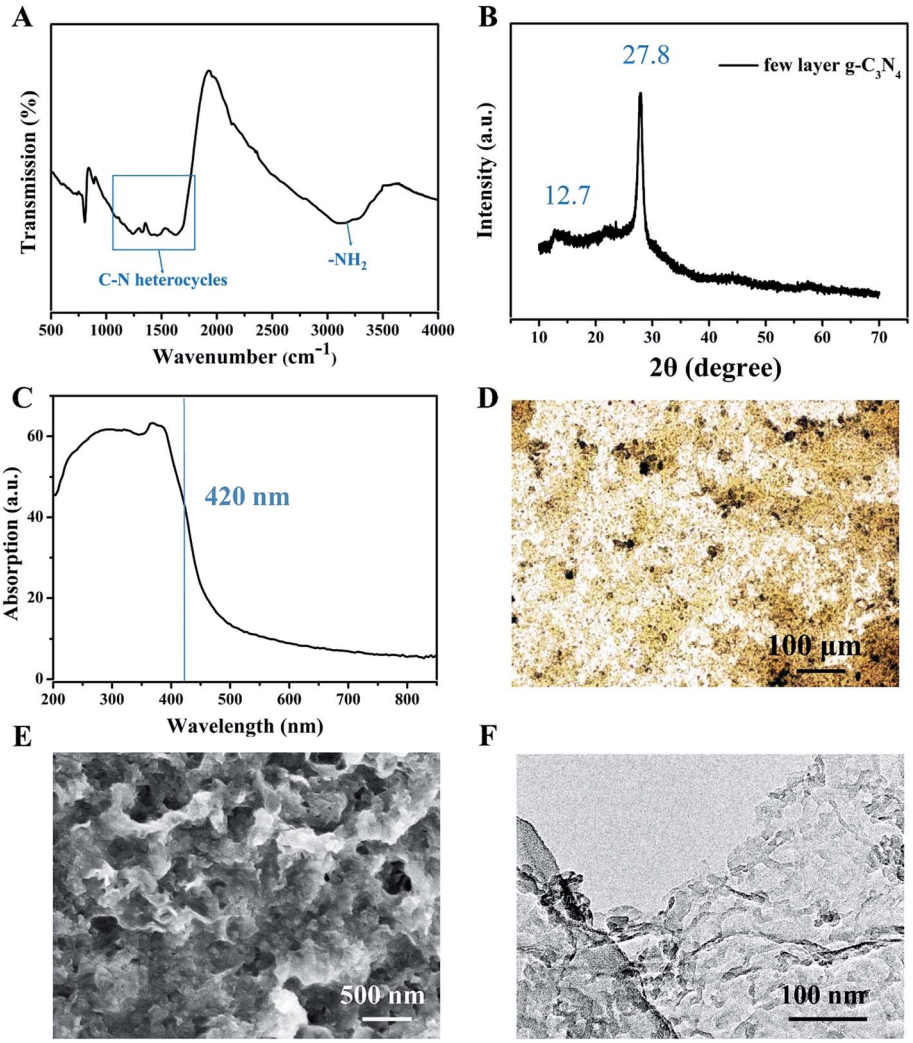

Fig. 2 Characterization of the few-layer g-C_3N_4 photocatalyst. (A) FTIR spectrum of the few-layer g-C_3N_4, showing typical C–N heterocycle stretches at 1251, 1325, 1419, 1571, and 1639 cm^{-1}, as well as the characteristic breathing mode of triazine units at 810 cm^{-1}. (B) XRD spectrum of the few-layer g-C_3N_4 with two peaks at 12.7° and 27.8°, ascribed to the lattice planes parallel to the *c*-axis and the stacking of the conjugated aromatic system, respectively. (C) UV-vis absorption spectrum of the few-layer g-C_3N_4. The blue line indicates the position of 420 nm. (D) The optical image of the IAPSI film. (E) The SEM image of the IAPSI film, in which the scale bar is 1 μm. (F) The TEM image of the few-layer g-C_3N_4 material.

image of the IAPSI is shown in Fig. 2D, and the corresponding enlarged structure by SEM is shown in Fig. 2E, from which we found that the few-layer g-C_3N_4 has a loose morphology. The TEM image (Fig. 2F) shows the graphene-like appearance of the few-layer g-C_3N_4, which is similar to previously published work.[34] As an important factor, the thickness of the few-layer g-C_3N_4 was measured using AFM and found to be about 1.6 nm, corresponding to about three layers of g-C_3N_4 (Fig. S1†).

3.2 Characterization of the electron mediator M

We compared the structural/chemical information of M in the traditional method and the one-step method by NMR. We obtained the correct structure in both methods, as shown in Fig. S2.† However, the one-step method saved time and reduced the chance to obtain impurities to some extent. The activity of the electron mediator M is of great importance. The reported method to detect the activity of M was the existence of the absorption peak at ~230 nm, corresponding to the bipyridine ligand.[38] Herein, we synthesized a series of M by the one-step method with different concentrations from 0.008 to 0.08 mM. As shown in Fig. 3A, the characteristic peaks at 232 nm, 304 nm and 312 nm are clear, proving the correct structure and the effective activity of the synthesized M. We then fitted these data and obtained good linearities between the M concentration and the absorption at the characteristic peaks (Fig. 3B). The correlation coefficient (R^2) in each line was around 0.999, and the slope was 37.68, 17.74 and 17.65 mM^{-1} for the peaks at 232 nm, 304 nm and 312 nm, respectively. We also obtained very similar UV-vis spectra after storage in the fridge for three months, showing good stability for M stored in ethanol. The line of 340 nm in Fig. 3A is not for M, instead it indicates the position of absorption peak of NADH. From Fig. 3B, it is seen that the absorption at 340 nm varies very little with an increase in the concentration of M.

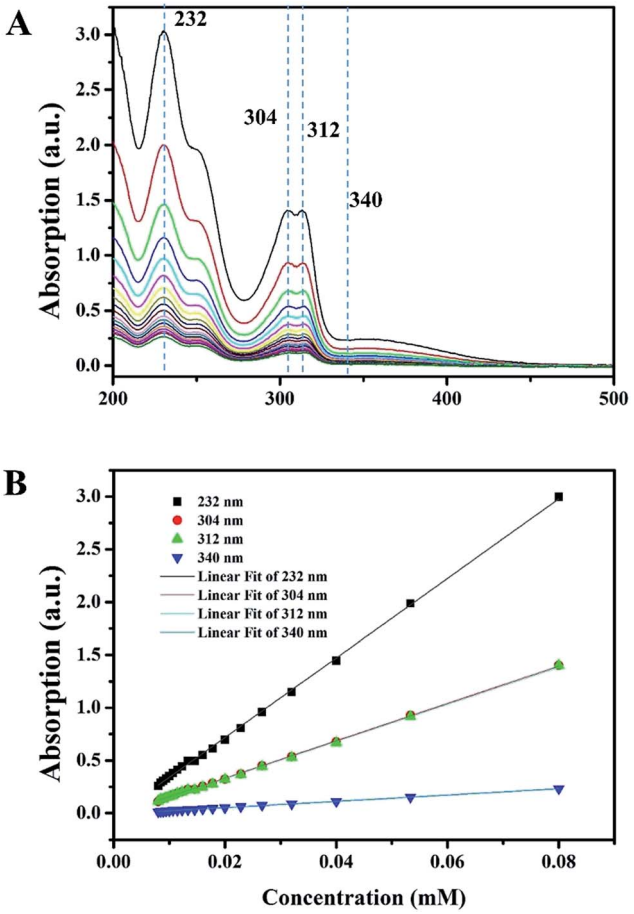

Fig. 3 UV-vis spectrum of M in the one-step method. (A) M in different concentrations and their characteristic peaks at 232 nm, 304 nm and 312 nm, proving the synthesized M with the correct structure and effective activity. Another peak at 340 nm indicates the position of the absorption peak of NADH. (B) Fitting the data resulted in good linearity between the concentration and the absorption at the characteristic peaks. The absorption change at 340 nm is very little with an increase in the concentration of M.

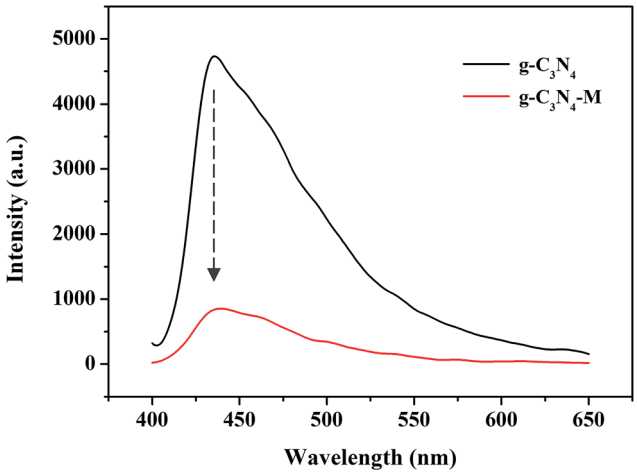

Fig. 4 The photoluminescence emission spectra of the few-layer g-C_3N_4 (black line) with the emission peak at 436 nm. With the addition of M, the emission peak obviously drops (red line), which directly proves an enhancement of the electron transfer from g-C_3N_4 to M.

After testing the activity of M, the coupling between g-C_3N_4 and M should also be verified because this is another critical factor that affects the catalytic performance. The interaction between g-C_3N_4 and M enables the hydride transfer from the excited conduction band of g-C_3N_4 to NAD^+ *via* the mediation of M. To directly detect and prove the electron transfer from g-C_3N_4 to M, we performed the PL assay. As shown in Fig. 4, a strong PL emission peak at 436 nm is observed for the few-layer g-C_3N_4 (black line), which can be attributed to the recombination of photo-induced electrons and holes. In contrast, the PL emission peak intensity of the few-layer g-C_3N_4 with M (red line) is much weaker than the former one, which directly proves an enhancement of the electron transfer from the g-C_3N_4 to M in the photocatalytic process.

3.3 NADH regeneration

We detected the NADH regeneration in three systems, which were the bulk g-C_3N_4–slurry system, the few-layer g-C_3N_4–slurry system and the IAPSI microreactor. The former two were used as the control to compare with the last one. The slurry systems were placed into a reflux condenser reactor equipped with a stirring bar and illuminated with a xenon lamp. The IAPSI microreactor was filled with the reaction solution and covered by a glass slide to avoid the water evaporation through the PDMS layer without stirring. Under similar conditions, previous studies in the microfluidic chip[39] reported a decrease in the regeneration rate with an increase in the flow rate. To avoid the influence of flow rate, we choose the static flow (*i.e.*, the flow rate is 0) in this work. Thus, the flow shear stress was not an influential factor. However, for the completeness of this research, we performed the shear stress test and presented the results in the ESI (see Fig. S3†). The distance between the IAPSI microreactor and the xenon lamp was fixed at 10 cm. Before the illumination, the reaction solution was placed in a dark environment for a sufficiently long time to achieve the adsorption–desorption equilibrium. Under the illumination, the concentration of NADH was calculated by measuring the absorption of the diluted reaction system at 340 nm. NADH had the peak absorption at 340 nm with an extinction coefficient of 6220 M^{-1} cm^{-1}. Fig. 5A shows the UV-vis spectrum changes of the bulk g-C_3N_4–slurry system within 4 hours, whereas Fig. 5B shows the data of the few-layer g-C_3N_4–slurry system over 90 min. Although the times are different, the regeneration rate reaches similar levels of 50% at 90 min (few-layer g-C_3N_4–slurry) and 47.9% at 4 hours (bulk g-C_3N_4–slurry). Thus, the regeneration rate in the few-layer g-C_3N_4–slurry system is much faster, showing good catalytic ability. This can be attributed to its porous structural feature, which contains more sites that are reactive and improves the light harvesting by inner scattering, leading to more photogenerated electron carriers. These electrons are subsequently transferred to M, and then shuffled to NAD^+ to regenerate 1,4-NADH.

In the IAPSI microreactor, the regeneration rate was much more satisfactory. As shown in Fig. 5C, the absorption at 340 nm

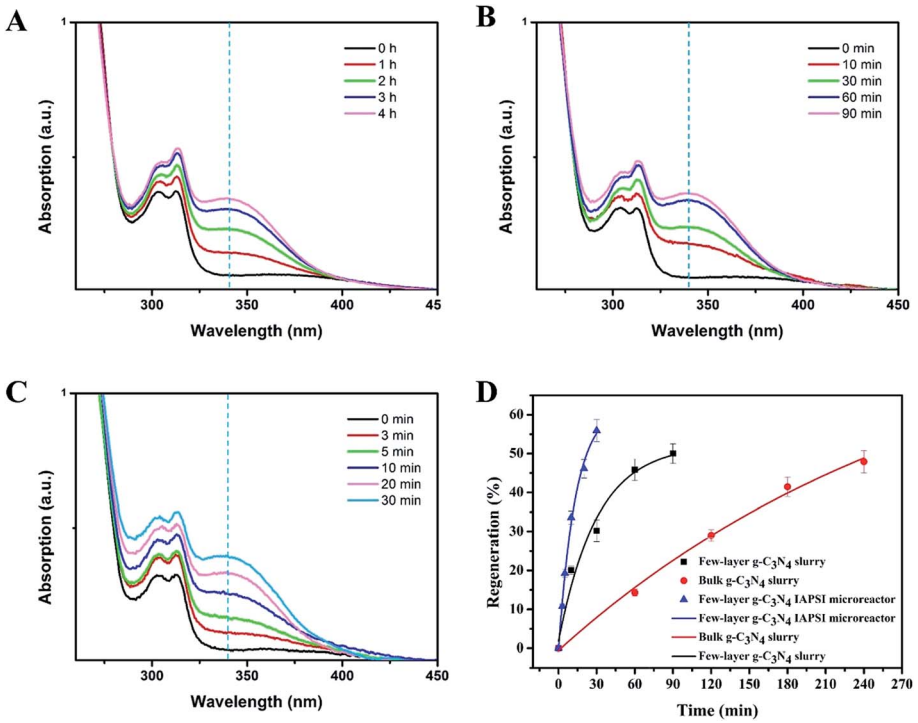

Fig. 5 Comparison of the NADH regeneration rates of the three systems by UV-vis spectral measurements of the NADH concentration with a lapse in time. Spectral changes of the bulk g-C_3N_4–slurry system (A), the few-layer g-C_3N_4–slurry system (B) and the few-layer g-C_3N_4-IAPSI microreactor (C). (D) Comparison of the regeneration percentage as a function of time for the three systems. The regeneration percentage reached 47.9% at 4 hours for the bulk g-C_3N_4–slurry system, 50% at 90 min for the few-layer g-C_3N_4–slurry system, and 11% at 3 min and 56% at 30 min for the few-layer g-C_3N_4-IAPSI microreactor. From the fitting curves in (D), it was found that the characteristic time of each was about 13 s (IAPSI), 30 s (few-layer g-C_3N_4–slurry system) and 305 s (bulk g-C_3N_4–slurry system). As a result, the IAPSI microreactor was ~2.3 times and ~23 times faster than the other two in terms of NADH regeneration.

rises to 10.8% at 3 min and 55.9% at 30 min. To compare the regeneration rate in the three systems (bulk g-C_3N_4–slurry, few-layer g-C_3N_4–slurry and IAPSI microreactor), we plotted the regeneration percentage as a function of time in Fig. 5D. The exponential relationship is $y = A \exp(-x/t_c) + y_0$, where t_c is the characteristic chemical time, defined as the time required for the concentration of A to fall from its initial value to a value equal to $1/e$ times the initial value. Calculated from Fig. 5D, the t_c values of the IAPSI microreactor, the few-layer g-C_3N_4–slurry system and the bulk g-C_3N_4–slurry system are 13 s, 30 s and 305 s, respectively, which means the IAPSI microreactor is about 2.3 times and 23 times faster than the others. The improvement of the regeneration rate is ascribed to three reasons: (1) high surface-area-to-volume ratio, (2) short diffusion length and (3) uniform irradiation in the IAPSI microreactor. In the future, we will study more factors that affect the regeneration results, such as oxygen, flow rate and temperature by integrating more control units into the IAPSI microreactor. Furthermore, we will try to scale up the microreactor and work with other enzymes for the production of high performance functional materials.[40–43]

4 Conclusion

In conclusion, we proposed a one-step method to form the immobilized artificial PSI (IAPSI) in a microfluidic chip. This method is advantageous over the traditional three-step method in by having a simple process, promotion of the g-C_3N_4 and M by π–π stacking and a high coenzyme regeneration rate. The advantages of this method create the potential for artificial photosynthesis in the future.

Acknowledgements

This work was supported by the National Science Foundation of China (no. 61377068), Research Grants Council (RGC) of Hong Kong (N_PolyU505/13, PolyU 5334/12E, and PolyU 152184/15E), and The Hong Kong Polytechnic University (G-YN07, G-YBBE, 4-BCAL, 1-ZVAW, 1-ZE14, A-PM21, 1-ZE27 and 1-ZVGH).

References

1 D. Gust, T. A. Moore and A. L. Moore, *Acc. Chem. Res.*, 2009, **42**, 1890–1898.
2 S. Berardi, S. Drouet, L. Francàs, C. Gimbert-Suriñach, M. Guttentag, C. Richmond, T. Stoll and A. Llobet, *Chem. Soc. Rev.*, 2014, **43**, 7501–7519.
3 S. Takeuchi, S. Ruhman, T. Tsuneda, M. Chiba, T. Taketsugu and T. Tahara, *Science*, 2012, **338**, 1321–1325.
4 M. Mifsud, S. Gargiulo, S. Iborra, I. W. C. E. Arends, F. Hollmann and A. Corma, *Nat. Commun.*, 2014, **5**, 3145.

5 H. Zhou, J. Guo, P. Li, T. Fan, D. Zhang and J. Ye, *Sci. Rep.*, 2013, **3**, 1667.
6 X. H. Li, J. Zhang, X. Chen, A. Fischer, A. Thomas, M. Antonietti and X. Wang, *Chem. Mater.*, 2011, **23**, 4344–4348.
7 X. Wang, K. Maeda, A. Thomas, K. Takanabe, G. Xin, J. M. Carlsson, K. Domen and M. Antonietti, *Nat. Mater.*, 2009, **8**, 76–80.
8 Y. Maenaka, T. Suenobu and S. Fukuzumi, *J. Am. Chem. Soc.*, 2012, **134**, 367–374.
9 J. Liu, N. P. Wickramaratne, S. Z. Qiao and M. Jaroniec, *Nat. Mater.*, 2015, **14**, 763–774.
10 J. Liu, Q. Zhang, J. Yang, H. Ma, M. O. Tade, S. Wang and J. Liu, *Chem. Commun.*, 2014, **50**, 13971–13974.
11 Z. Y. Zhao, J. Liu, M. Hahn, S. Qiao, A. P. J. Middelberg and L. He, *RSC Adv.*, 2013, **3**, 22008–22013.
12 Y. Zheng, J. Liu, J. Liang, M. Jaroniec and S. Z. Qiao, *Energy Environ. Sci.*, 2012, **5**, 6717–6731.
13 H. Zhou, X. Li, T. Fan, F. E. Osterloh, J. Ding, E. M. Sabio, D. Zhang and Q. Guo, *Adv. Mater.*, 2010, **22**, 951–956.
14 J. Barber, *Chem. Soc. Rev.*, 2009, **38**, 185–196.
15 J. Liu and M. Antonietti, *Energy Environ. Sci.*, 2013, **6**, 1486–1493.
16 F. Wang, W. G. Wang, X. J. Wang, H. Y. Wang, C. H. Tung and L. Z. Wu, *Angew. Chem., Int. Ed.*, 2011, **50**, 3193–3197.
17 J. Ryu, S. H. Lee, D. H. Nam and C. B. Park, *Adv. Mater.*, 2011, **23**, 1883–1888.
18 C. Luo, D. M. Guldi, H. Imahori, K. Tamaki and Y. Sakata, *J. Am. Chem. Soc.*, 2000, **122**, 6535–6551.
19 S. H. Lee, J. Ryu, D. H. Nam and C. B. Park, *Chem. Commun.*, 2011, **47**, 4643–4645.
20 J. Huang, M. Antonietti and J. Liu, *J. Mater. Chem. A*, 2014, **2**, 7686–7693.
21 J. Liu, R. Cazelles, Z. P. Chen, H. Zhou, A. Galarneau and M. Antonietti, *Phys. Chem. Chem. Phys.*, 2014, **16**, 14699–14705.
22 N. Wang, X. Zhang, Y. Wang, W. Yu and H. L. W. Chan, *Lab Chip*, 2014, **14**, 1074–1082.
23 T. M. Squires and S. R. Quake, *Rev. Mod. Phys.*, 2005, **77**, 977–1026.
24 G. M. Whitesides, *Nature*, 2006, **442**, 368–373.
25 X. Huang, W. Hui, C. Hao, W. Yue, M. Yang, Y. Cui and Z. Wang, *Small*, 2014, **10**, 758–765.
26 J. Liu, Y. Liu, N. Liu, Y. Han, X. Zhang, H. Huang, Y. Lifshitz, S. Lee, J. Zhong and Z. Kang, *Science*, 2015, **347**, 970–974.
27 Z. Zhou, Y. Shen, Y. Li, A. Liu, S. Liu and Y. Zhang, *ACS Nano*, 2015, **9**, 12480–12487.
28 J. Liu, H. Wang and M. Antonietti, *Chem. Soc. Rev.*, 2016, **45**, 2308–2326.
29 J. Duan, S. Chen, M. Jaroniec and S. Z. Qiao, *ACS Nano*, 2015, **9**, 931–940.
30 Z. Meng, X. Zhang and J. Qin, *Nanoscale*, 2013, **5**, 4687–4690.
31 M. Poizat, I. W. C. E. Arends and F. Hollmann, *J. Mol. Catal. B: Enzym.*, 2010, **63**, 149–156.
32 K. T. Oppelt, J. Gasiorowski, D. A. M. Egbe, J. P. Kollender, M. Himmelsbach, A. W. Hassel, N. S. Sariciftci and G. Knör, *J. Am. Chem. Soc.*, 2014, **136**, 12721–12729.
33 Y. Liu, L. Moevius, X. Xu, T. Qian, J. M. Yeomans and Z. Wang, *Nat. Phys.*, 2014, **10**, 515–519.
34 P. Niu, L. Zhang, G. Liu and H. M. Cheng, *Adv. Funct. Mater.*, 2012, **22**, 4763–4770.
35 D. C. Duffy, J. C. McDonald, O. J. A. Schueller and G. M. Whitesides, *Anal. Chem.*, 1998, **70**, 4974–4984.
36 X. Huang, Y. Zhu, X. Zhang, Z. Bao, D. Y. Lei, W. Yu, J. Dai and Y. Wang, *Sens. Actuators, B*, 2016, **222**, 106–111.
37 H. H. Zhao, H. Yu, X. Quan, S. Chen, Y. Zhang, H. H. Zhao and H. Wang, *Appl. Catal., B*, 2014, **152–153**, 46–50.
38 F. Hollmann, B. Witholt and A. Schmid, *J. Mol. Catal. B: Enzym.*, 2002, **19–20**, 167–176.
39 J. S. Lee, S. H. Lee, J. H. Kim and C. B. Park, *Lab Chip*, 2011, **11**, 2309–2311.
40 X. Huang, W. Yue, D. Liu, J. Yue, J. Li, D. Sun, M. Yang and Z. Wang, *Sci. Rep.*, 2016, **6**, 23591.
41 S. Choudhury, J. O. Baeg, N. J. Park and R. K. Yadav, *Angew. Chem., Int. Ed.*, 2012, **51**, 11624–11628.
42 H. C. Lo and R. H. Fish, *Angew. Chem., Int. Ed.*, 2002, **41**, 478–481.
43 P. Könst, H. Merkens, S. Kara, S. Kochius, A. Vogel, R. Zuhse, D. Holtmann, I. W. C. E. Arends and F. Hollmann, *Angew. Chem., Int. Ed.*, 2012, **51**, 9914–9917.